ENVIRONMENTAL STUDIES

Long-term viability of carbon sequestration in deep-sea sediments

Yihua Teng[1,2] and Dongxiao Zhang[3]*

Sequestration of carbon dioxide in deep-sea sediments has been proposed for the long-term storage of anthropogenic CO_2 that can take advantage of the current offshore infrastructure. It benefits from the negative buoyancy effect and hydrate formation under conditions of high pressure and low temperature. However, the multiphysics process of injection and postinjection fate of CO_2 and the feasibility of subseabed disposal of CO_2 under different geological and operational conditions have not been well studied. With a detailed study of the coupled processes, we investigate whether storing CO_2 into deep-sea sediments is viable, efficient, and secure over the long term. We also study the evolution of multiphase and multicomponent flow and the impact of hydrate formation on storage efficiency. The results show that low buoyancy and high viscosity slow down the ascending plume and the forming of the hydrate cap effectively reduces permeability and finally becomes an impermeable seal, thus limiting the movement of CO_2 toward the seafloor. We identify different flow patterns at varied time scales by analyzing the mass distribution of CO_2 in different phases over time. We observe the formation of a fluid inclusion, which mainly consists of liquid CO_2 and is encapsulated by an impermeable hydrate film in the diffusion-dominated stage. The trapped liquid CO_2 and CO_2 hydrate finally dissolve into the pore water through diffusion of the CO_2 component, resulting in permanent storage. We perform sensitivity analyses on storage efficiency under variable geological and operational conditions. We find that under a deep-sea setting, CO_2 sequestration in intact marine sediments is generally safe and permanent.

INTRODUCTION

Carbon capture and storage is considered as a promising option to stabilize the atmospheric concentration of anthropogenic CO_2 and mitigate climate change (*1*, *2*). Conventional proposals for geologic sequestration, including injection into deep saline aquifers, oil and gas fields, and deep coal seams, are prospective, but the stored supercritical CO_2 is buoyant and consequently may escape via permeable pathways into the atmosphere (*3*, *4*). In contrast, liquid CO_2 can be denser than seawater and become gravitationally stable at high pressure and low temperature, which is typical in deep-sea settings. Metz *et al.* (*5*) have proposed direct injection of CO_2 into the deep ocean because of the relatively high solubility of CO_2 into seawater and negative buoyancy, which results in liquid CO_2 becoming a sinking plume and finally forming a CO_2 lake on the seafloor (*6*–*8*). While the great residence time of this means increases in storage efficiency and the enormous volume of the ocean guarantees storage capacity, it suffers from disturbance of ocean currents and negative impacts on the marine environment (*9*).

A viable alternative is to store liquid CO_2 in deep-sea sediments (*10*–*13*). This option shares the advantages of ocean storage but is free from potential hazards to the ocean system. The major trapping mechanisms in terrestrial sequestration, such as residual trapping, dissolution trapping, and mineral trapping, still apply under this scenario. The pressure and temperature conditions of the negative buoyancy zone (NBZ), which extends from the seafloor downward to the neutrally buoyant level, provides a buoyancy cap and is referred to as gravitational trapping (*11*). Within the sediment, the existence of a hydrate-forming zone (HFZ), where CO_2 hydrate is stable at prevailing high pressure and low temperature, leads to hydrate trapping (*12*, *14*). The formation of hydrate clogs pore space and serves as an impermeable cap, thus impeding the upward flow of injected CO_2. On the other hand, the hydrate itself traps CO_2 in its crystal structure, which constitutes another way of storing CO_2.

Figure 1 shows the schematic of the related processes and infrastructure of sequestering CO_2 into deep-sea sediments. The required infrastructure is similar to that used in the recent production pilot of natural gas hydrate extraction in the South China Sea (*15*). Sequestration of CO_2 can also be combined with methane hydrate production through either simultaneous CO_2 injection or injecting CO_2 into the depleted gas hydrate reservoirs (*16*). Here, we mainly focus on injecting CO_2 into the deep-sea sediments without the existence of natural gas hydrate. The captured CO_2 is transported through pipelines or ships to the platform and then injected into the sediments beneath the seafloor. After injection, the buoyant CO_2 gradually loses heat during floating and then forms hydrate or becomes gravitationally stable. After the CO_2 plume stops moving upward, the increased density of the surrounding pore fluid due to the dissolution of CO_2 (*17*) will lead to the sinking of the CO_2-saturated fluid. In the long term, diffusion will dominate, transforming all of the liquid CO_2 and CO_2 hydrate into CO_2 solution. Effectively evaluating the viability of subseabed sequestration requires an accurate description of the multiphysics process of CO_2 transport in the porous sediment, including multiphase and multicomponent flow, nonisothermal effect due to heat flow, chemical reaction due to potential hydrate formation and dissociation, and dynamics of dissolved components. Previous studies have investigated the effectiveness of CO_2 storage in ocean sediments theoretically, experimentally, and numerically (*18*–*24*), but none of them fully coupled the related physical processes. Specifically, models in the previous studies did not consider the dissolved species. However, incorporation of dissolved components and their corresponding effects on hydrate reaction and fluid flow is the key to studying the long-term evolution of different phases and components, such as density-driven convection and dissolution of

[1]Department of Energy and Resources Engineering, College of Engineering, Peking University, Beijing 100871, China. [2]Institute of Ocean Research, Peking University, Beijing 100871, China. [3]Beijing Innovation Center for Engineering Science and Advanced Technology, Department of Energy and Resources Engineering, and State Key Laboratory for Turbulence and Complex Systems, College of Engineering, Peking University, Beijing 100871, China.
*Corresponding author. Email: dxz@pku.edu.cn

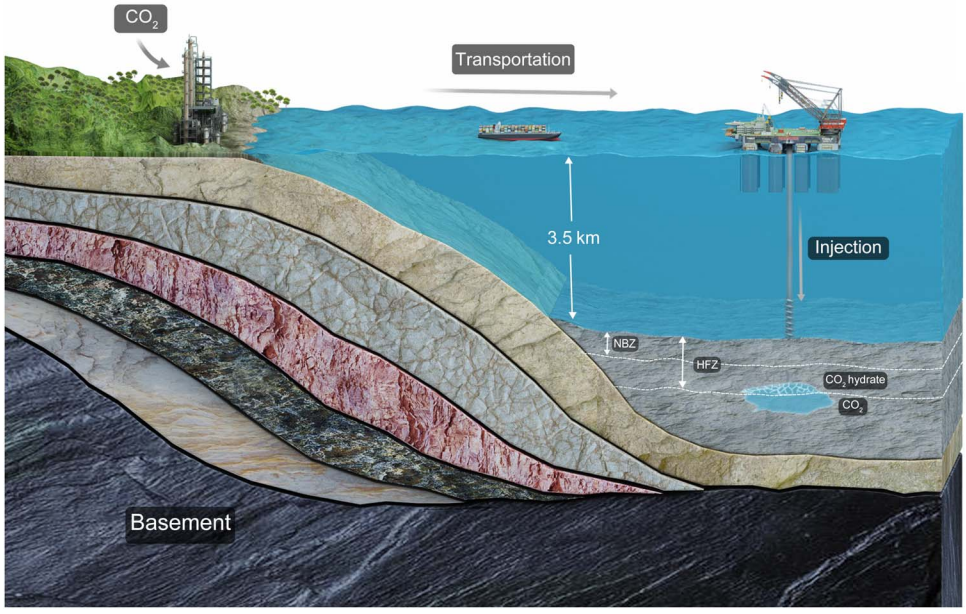

Fig. 1. Schematic illustration of carbon sequestration in deep-sea sediments. The captured CO_2 is transported through ships to the platform and then injected into the submarine sediments.

liquid CO_2 and hydrate. Consequently, there is a lack of discussion about the long-term fate of the injected CO_2. Here, on the basis of an integrated model, we investigate the short-term and long-term fate of injected CO_2 and analyze the viability of CO_2 storage in deep-sea sediments under different geologic and operational conditions.

RESULTS

Important phenomena and long-term viability

To gain insight into the major processes and trapping mechanisms of sequestration in deep-sea sediments, we set up the base case according to the deep ocean setting with an ocean depth of approximately 3500 m. In the base case, the pressure and temperature at the seafloor are 35 MPa and 3°C, respectively, with a geothermal gradient of 0.03 K/m (see the Supplementary Materials for additional details). The thickness of the HFZ and NBZ is 344 and 225 m, respectively. The sediment is homogeneous but anisotropic, with a vertical permeability of 10 mD and a horizontal permeability of 50 mD. The simulation domain is a cylindrical system with a radius of 10 km.

In the base case, liquid CO_2 is injected into the homogeneous sediment at a depth of 400 m below the seafloor for 10 years. The injection rate is 750 metric tons/day, and a total of 2.7375 million tons of CO_2 are injected into the sediment at the end of injection. Figure 2 shows the spatial distribution of different variables at different times. Each subplot is a cross-sectional view of the three-dimensional (3D) cylindrical system. r and z axes represent horizontal and vertical direction, respectively, and the location of the seafloor is at $z = 0$. Different from a terrestrial setting, the footprint of CO_2 is ellipsoidal, resulting from the low buoyancy compared to viscous force. Because of overpressure owing to injection, liquid CO_2 moves upward into the HFZ and disturbs the pressure and temperature profile. Hydrate begins to form as the front of the CO_2 plume gradually loses heat and reaches the equilibrium temperature for hydrate formation. At the end of the injection, there is a trace amount of hydrate formed at a certain distance above the base of the HFZ (Fig. 2A).

After injection, the expansion of the footprint slows down as the overpressure dissipates over time. During the upward movement of liquid CO_2 driven by buoyancy, hydrate continues to form and reduces the permeability of the sediment, thus slowing down the migration rate of the plume front (Fig. 2B). The increase of salinity at the plume front results from hydrate formation that extracts water from the pore fluid (Fig. 2Q). The higher salinity and heat release due to hydrate formation and dissolution of CO_2 into the aqueous phase, in turn, inhibit the formation of hydrate. Consequently, hydrate formation stops when salinity becomes high enough so that the hydrate formation temperature reduces to the local temperature (Fig. 2R). At $t = 246$ years, we observe the development of instability at the lower boundary of the footprint (Fig. 2L) due to the density difference between the CO_2-saturated fluid and the CO_2-unsaturated fluid, induced by CO_2 dissolution (*25*–*27*). At this time, because of permeability reduction, the rate of upward flow driven by buoyancy is similar to that of density-driven gravitational convection at the bottom.

The plume front continues to rise until it sufficiently cools down and leads to the formation of a hydrate film with saturation up to 0.95 (Fig. 2C). This hydrate film acts like a caprock with the effective permeability being lower than 3×10^{-4} mD. As time passes, the buoyant CO_2 accumulates under the impermeable hydrate cap and flows laterally, thus extending the edge of the cap (Fig. 2I). At this time scale, the downward flow of the CO_2-saturated pore fluid dominates. It mixes with the surrounding pore fluid and develops fingering. The entraining of pore water accelerates the conversion of liquid CO_2 to dissolved CO_2 (*28*, *29*). As the plume gradually loses heat, hydrate begins to form at the periphery of the plume and grows inward along the base of the HFZ (Fig. 2D). The CO_2-saturated solution creates a channel at the center, and a strong effect of fingering can be observed (Fig. 2N). Since the finger continues to mix with the surrounding unsaturated aqueous phase, which reduces its density, the later-formed finger catches up with the previous-formed finger and connects with it. In the long term, up to approximately 10^5 years, the shrinkage of the hydrate cap becomes obvious. The hydrate cap continues to close radially inward, seals the bottom of the plume,

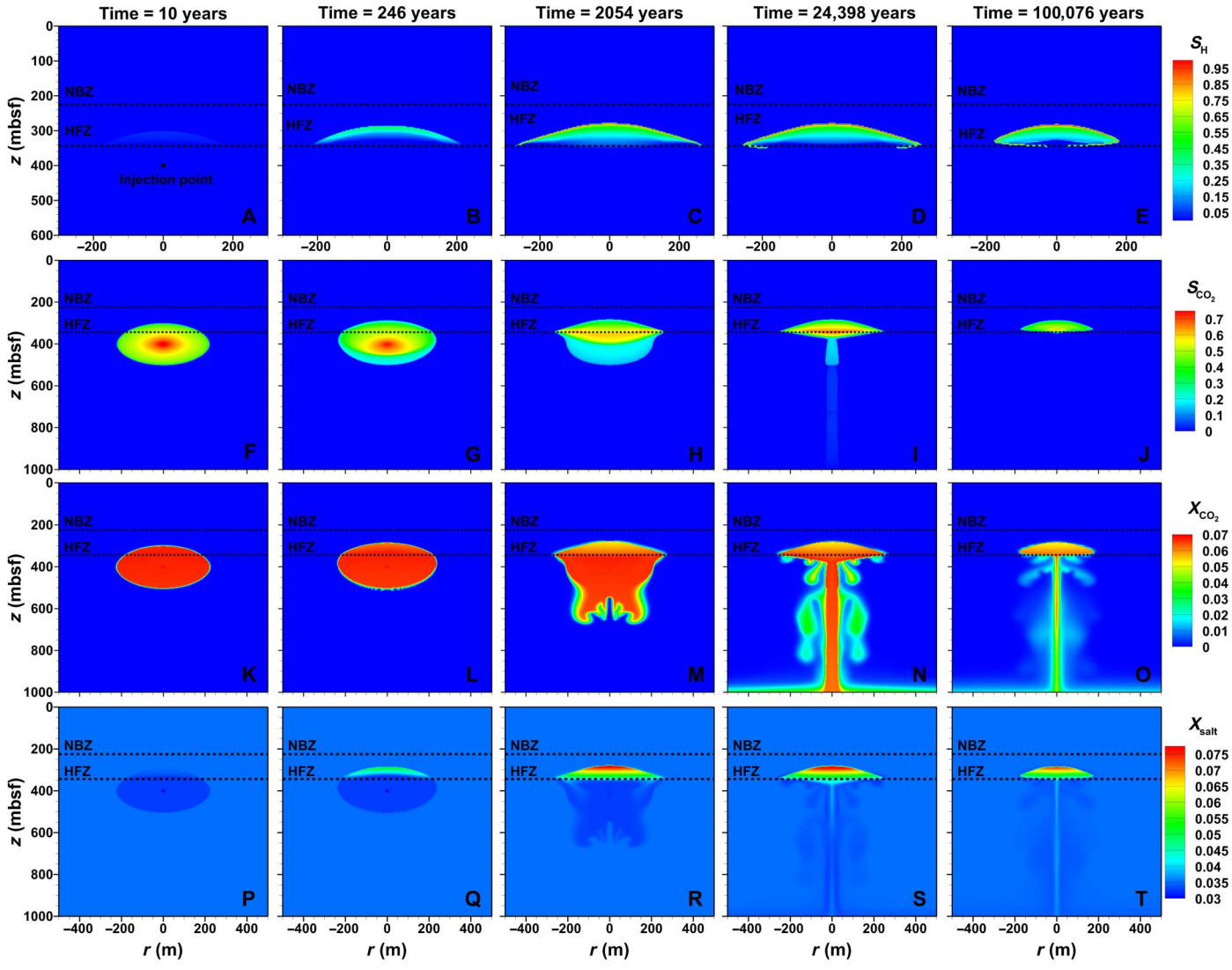

Fig. 2. Spatial distribution of different variables at specific times. (**A** to **E**) Saturation of CO_2 hydrate. (**F** to **J**) Saturation of liquid CO_2. (**K** to **O**) Mass fraction of component CO_2 in the aqueous phase. (**P** to **T**) Mass fraction of salt in the aqueous phase. The time of each column is the same and specified at the top of the figure.

and traps most of the liquid CO_2 inside it (Fig. 2, E and J). The density-driven downward flow is limited at the narrow channel at the center, and the fingering becomes much weaker (Fig. 2O). As hydrate formation continues to seal the bottom of the plume, a CO_2 fluid inclusion is formed. It is a cage-like system containing mainly liquid CO_2 that is not able to form hydrate due to the limited source of water and high salinity. After this, diffusion driven by the concentration gradient of dissolved CO_2 gradually dominates. The effect of diffusion can be observed through the slight increase of the mass fraction of dissolved CO_2 at the flank of the hydrate cap. The dissolved CO_2 at the interface of hydrate and water slowly diffuses into the surrounding pore fluid, thus leading to the dissolution and further shrinkage of the hydrate cap. Eventually, CO_2 hydrate and the remaining CO_2 (l) phase vanish and convert to the aqueous phase. Movies S1 to S4 show the detailed time evolution of the spatial distribution of the four parameters.

Figure 3 shows the mass distribution of the CO_2 component in different phases. The CO_2 component resides in the liquid CO_2 phase, the hydrate phase, and the aqueous phase. We identified four distinct stages during the whole process. Stage 1 starts from the end of the injection to approximately 200 years in which the buoyancy-driven upward flow of liquid CO_2 dominates, with a slight decrease of liquid CO_2 transforming to CO_2 hydrate and dissolved CO_2. Stage 2 is a transitional stage, with hydrate formation impeding the buoyant flow and the onset of instability at the bottom of the plume. In stage 3, the sinking of CO_2-saturated pore fluid dominates. The mixing of downward flow with the unsaturated pore fluid and the development of fingering accelerate the transformation of CO_2 from the CO_2-rich phase to the aqueous phase. This stage lasts as liquid CO_2 continues to dissolve into water until an impermeable hydrate film forms. At the end of stage 3, only approximately 10% of the total mass of the injected CO_2 resides in the liquid CO_2 phase, with most of the rest in the form of dissolved CO_2, and the time scale is approximately 10^5 years. As the formation of hydrate along the base of the HFZ continues to seal the bottom of the plume, diffusion gradually becomes the major flow type, and then stage 4 begins. The hydrate phase, together with the liquid CO_2 phase, slowly vanishes through diffusion and the continuous

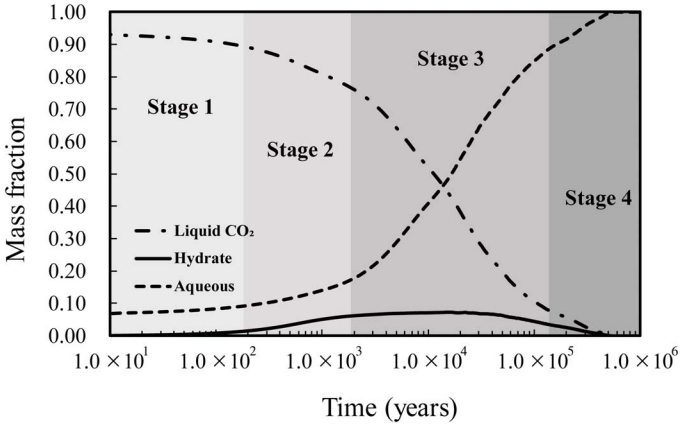

Fig. 3. Time evolution of the mass distribution of the CO_2 component in different phases. The value is defined by the ratio of the total mass of the CO_2 component in a specific phase to the total mass of injected CO_2. The dashed-dotted line represents the liquid CO_2 phase. The solid line represents the hydrate phase. The dashed line represents the aqueous phase.

dissolution of the CO_2 component into the aqueous phase. Figure 3 also shows that the CO_2 hydrate does trap CO_2, but the mass fraction of the CO_2 component in the hydrate phase is lower than 10% during the entire process. This means that hydrate mainly serves as a cap.

Viability under different geological and operational conditions

In this section, we carefully design parameters according to potential natural settings and possible operational conditions and investigate how these variables affect storage efficiency and viability. In addition to the base case, we run another 22 simulations. Table 1 shows the values of the parameters and the corresponding results. In each case, the specified parameter takes the corresponding value, with the rest being the same as those in the base case. The thickness of the HFZ and NBZ represents their ability to impede the upward flow of the buoyant CO_2 and is dependent on the natural environment, including ocean depth, seafloor temperature, geothermal gradient, and salinity. We recorded five parameters to describe the safety and storage efficiency at specific geological conditions or operational conditions. Here, we assume that the sediment is intact and no fracture or highly permeable conduit exists during the whole process.

There is no NBZ for a shallower ocean with depths of 1000 and 2000 m. The decrease of pressure results in lower CO_2 density and lower viscosity, thus leading to higher buoyancy and higher mobility. An increase in mobility can enlarge the footprint of the injected CO_2 (*21*), as proven by the smaller distance between the seafloor and the front of the CO_2 plume at the end of the injection (d_{PI}) with decreasing ocean depth. Increased buoyancy facilitates the upward flow of CO_2 toward the seafloor, giving rise to the risk of leakage. For sediments with larger permeability, the injected CO_2 moves further into the HFZ and resides just below the base of NBZ for the case of 100 mD. A higher value of the Carman-Kozeny factor (eq. S2) indicates a stronger effect of permeability reduction caused by hydrate formation, thereby reducing d_{min}, the minimum distance between the seafloor and the plume front. Since porosity represents the available void space for storing CO_2, the footprint of CO_2 is a decreasing function of porosity. Smaller porosity leads to further movement of the CO_2 plume into the HFZ. A slight change in temperature profile can cause a significant change in the HFZ and NBZ. In general, an increase in the prevailing temperature in the sediment shrinks the HFZ and NBZ. Therefore, an increase in either geothermal gradient or seafloor temperature reduces the impedance exerted on the buoyant CO_2, as proven by smaller d_{min} with higher geothermal gradient or seafloor temperature (Table 1).

For injection in the deeper part of the sediment, the injected CO_2 has a longer pathway to migrate. As a consequence, a larger amount of CO_2 becomes trapped as a residual phase due to capillary pressure. The sediment column below the base of the HFZ decelerates the CO_2 plume as it decreases CO_2 saturation and cools down the plume. For an injection depth of 500 meters below seafloor (mbsf), the plume front halts just at 9 m above the base of the HFZ. The plume with a larger injection rate penetrates further into the HFZ due to a larger overpressure that causes a stronger disturbance to the static condition of pressure and temperature. Similarly, a longer injection time stores more CO_2, and the plume front stops rising at a shallower location, where the effect of overpressurization becomes sufficiently weak to allow the formation of an impermeable hydrate cap. However, the effect of injection temperature is not obvious. This implies that a higher injection temperature can be used to avoid potential hydrate formation around the well due to large injection pressure.

For a deep-sea setting, once the injection stops, the distance of upward migration of CO_2 in the HFZ is very limited because of hydrate formation and low buoyancy as the plume gradually cools down. Consequently, for most cases, the front of the plume never reaches the NBZ. For an ocean depth equal to 3500 m, the nearest distance occurs in the case of a 100-year injection with d_{min} = 161 m. d_{up} at the last column is the distance of upward migration of the CO_2 plume after injection stops and generally represents the capability of the HFZ and NBZ to hinder the upward flow after injection. d_{HFZ} measures the maximum distance that the plume front moves past the base of the HFZ. The general low value of d_{up} reveals the important role of the HFZ and NBZ in the subseabed disposal of CO_2. The existence of a high value of d_{up} is attributed to the plume front not reaching the base of the HFZ at the end of the injection. In this case, d_{HFZ} has low values, except for cases of a shallower sea, which again reflects the strong impedance of the HFZ on buoyant flow in deep oceans. By definition, T_d indicates the time that it takes the CO_2 plume to stop floating. The value of T_d depends on the interaction of the injected CO_2, the original pore fluid, and the sediment column, and its determination is relatively complex. T_d, for most cases, is in the range of several hundred to approximately 1000 years. Its time scale is similar to that of the transitional stage in which the formation of hydrate drastically reduces the effective permeability of the sediment. The distance of CO_2 migration in the sediment depends on the driving force and the ability of the sediment to conduct fluid flow. The driving force comes from buoyancy and the overpressurization of injection. Therefore, we can find that either shallower ocean depth or larger overpressure will lead to further migration of CO_2 toward the seafloor. The formation of hydrate requires liquid CO_2 to cool down enough so that its temperature falls below the temperature of hydrate formation. If the upward flow is too fast, then the buoyant CO_2 may not be sufficiently cooled and consequently penetrates the sediment to the seafloor. In the setting of a shallower sea with high vertical permeability, the formation of hydrate cannot sufficiently impede the buoyant CO_2, and thus, leakage occurs. Nevertheless, for storage in deep-ocean sediments, we observe no leakage under various scenarios.

DISCUSSION

In summary, by systematically studying the coupled process and how the system evolves under complex interactions between phases and

Table 1. Results of the sensitivity study. L_{HFZ}, thickness of HFZ; L_{NBZ}, thickness of NBZ; d_{PI}, distance between the seafloor and the front of the CO_2 plume at the end of the injection; d_{min}, minimum distance between the seafloor and the front of the CO_2 plume; T_d, time spent for the CO_2 plume to reach the minimum distance; d_{HFZ}, distance between the front of the CO_2 plume and the base of HFZ at T_d; d_{up}, distance of upward migration of the CO_2 plume after injection ceases.

Parameters	Value	L_{HFZ} (m)	L_{NBZ} (m)	d_{PI} (m)	d_{min} (m)	T_d (years)	d_{HFZ} (m)	d_{up} (m)
Ocean depth (m)	1000	252	—	287	29	2742	223	258
	2000	295	—	293	107	4698	188	186
	3500*	344	225	299	281	363	63	18
Vertical permeability (mD)†	10*	344	225	299	281	363	63	18
	50	344	225	299	251	267	93	48
	100	344	225	293	227	272	117	66
Vertical permeability (mD) with ocean depth = 1000 m	10	252	—	287	29	2742	223	258
	50	252	—	257	0	189	252	257
	100	252	—	227	0	89	252	227
Geothermal gradient (K/m)	0.03*	344	225	299	281	363	63	18
	0.04	259	153	299	233	1038	26	66
	0.05	206	116	299	197	970	9	102
Seafloor temperature (°C)	3*	344	225	299	281	363	63	18
	4	315	178	299	269	771	46	30
	5	280	131	299	257	818	23	42
Carman-Kozeny factor	3*	344	225	299	281	363	63	18
	5	344	225	299	292	235	52	7
	7	344	225	299	298	79	46	1
Porosity	0.15	344	225	281	263	268	81	18
	0.25*	344	225	299	281	363	63	18
	0.35	344	225	311	293	394	51	18
Injection depth (mbsf)	350	344	225	251	239	344	105	12
	400*	344	225	299	281	363	63	18
	500	344	225	401	335	1150	9	66
Injection rate (metric tons/day)	750*	344	225	299	281	363	63	18
	1500	344	225	275	251	673	93	24
	2250	344	225	257	233	595	111	24
Injection time (years)	10*	344	225	299	281	363	63	18
	50	344	225	233	209	543	135	24
	100	344	225	191	161	1009	183	30
Injection temperature (°C)	15*	344	225	299	281	363	63	18
	20	344	225	299	275	473	69	24
	25	344	225	299	269	603	75	30

*Base case. †For the case of changing vertical permeability, the ratio of horizontal permeability to vertical permeability remains the same (5:1) to ensure the same anisotropy.

components, we investigate the viability of sequestration in deep-sea sediments under different conditions and provide valuable insights into this problem. Compared with previous studies (*19*, *21*, *24*), we take different mechanisms into account, including the dynamics of dissolved components and their corresponding effects on hydrate formation and fluid flow, which is the prerequisite for the description of density-driven convection, dissolution of liquid CO_2 and CO_2 hydrate, and diffusion of dissolved CO_2 during the long-term evolution of the system. Because of a lack of consideration of dissolved components, most previous studies are limited to short-term processes. The incorporation of dissolved species and their related impacts enables us to predict the long-term fate of the injected CO_2 and consequently analyze the effectiveness and feasibility of this option. Our results demonstrate that in intact deep-sea sediments, the formation of the hydrate cap and the low buoyancy, or even negative buoyancy, effectively immobilize the injected CO_2, which makes this option a safe storage. The hydrate cap seals the periphery of the plume and traps the remaining liquid CO_2 in a cage-like system. The limited sources of water and the increased salinity due to hydrate formation prevent further formation of hydrate inside the fluid inclusion. Although diffusion of CO_2 into the surrounding pore fluid induces dissolution of the impermeable hydrate film at the periphery of the plume, we observe no leakage during the whole process. Instead, the impermeable hydrate film moves inward and continues to trap the liquid CO_2 inside it. Over time, both CO_2 hydrate and liquid CO_2 will totally dissolve into the surrounding pore fluid and transform into dissolved CO_2, which is more stable and less susceptive to geologic perturbation. Finally, the dissolved CO_2 migrates away through diffusion. The final dissolution of CO_2 hydrate and liquid CO_2 and the dilution of the CO_2-saturated fluid due to diffusion and convective mixing lead to permanent storage. The short-term immobilization of CO_2 by the hydrate cap and negative buoyancy and the long-term dissolution of CO_2 hydrate and liquid CO_2 ensure the long-term viability of sequestration in deep-sea sediments. During the whole process, the general low mass fraction of the CO_2 component in the hydrate phase implies that when a large amount of CO_2 is injected into deep-sea sediments, the CO_2 hydrate mainly serves as a cap to prevent the upward flow of buoyant CO_2, rather than being a major mechanism of storing CO_2. The results of the sensitivity study indicate that larger ocean depth, smaller vertical permeability, and cooler environment are favorable for CO_2 sequestration in submarine sediments. The limited travel distance of the buoyancy-driven flow of CO_2 in the HFZ reveals that hydrate formation and decreased buoyancy effectively impede the floating CO_2.

Under a deep-sea setting, the high density and viscosity of CO_2 result in a small footprint and, thus, high storage efficiency. This ensures great storage potential due to the wide distribution of deep-sea sediments globally. Compared with terrestrial sequestration, less lateral expansion reduces the possibility of CO_2 reaching a potential permeable pathway to the seafloor. The generation of a hydrate cap and the possible negative buoyancy make this option free from reliance on the caprock in terrestrial storage. In our assumption, the unconsolidated marine sediment is intact. However, faults or fractures may preexist in the sediment or be induced by tectonism or excessive injection overpressure that may create a permeable pathway directly to the seafloor. Under proper conditions, this system may generate a conduit of local three-phase equilibrium with hydrate formation (*30*, *31*), which allows upward migration of buoyant CO_2 to the seafloor. It is also possible that the formation of hydrate seals the permeable channel and prevents leakage. Whether CO_2 will escape or be trapped depends on the interaction of the competing processes of buoyant flow, hydrate formation, and density increase of CO_2 induced by heat loss. This issue is subject to further study to evaluate what conditions lead to what scenarios. In general, heterogeneity of the sediments, which mainly depends on the depositional environment and tectonism in the sedimentary history, may have a considerable impact on injectivity, spatial distribution and frontal movement of the CO_2 plume, density-driven convective mixing, and storage capacity (*32*–*36*). Stratigraphic heterogeneity, such as layered sediments, may defer the upward migration of CO_2 by several less permeable layers and enhance lateral spreading of the CO_2 plume, consequently leading to more dissolution trapping by the increasing contact of CO_2 and pore fluid (*37*, *38*). Even small-scale heterogeneity within a depositional facies can cause trapping of CO_2 and induce ramified displacement fronts due to local capillary heterogeneity (*39*, *40*). In our problem, assuming heterogeneous submarine sediments may change the way of expansion and migration of the plume and result in different spatial distributions of hydrate saturation and therefore various shapes of hydrate cap. It may also affect convective mixing at the bottom of the plume, as well as diffusion in the long term, thus giving different time evolutions of mass distribution of the CO_2 component in each phase. However, moderate heterogeneity is not likely to change the fundamental conclusion that this option constitutes safe and permanent storage, according to the results of various permeabilities and porosities in our sensitivity study. Nevertheless, additional investigation is necessary to obtain more insights into the effect of heterogeneity on CO_2 sequestration in deep-sea sediments. Since the whole system is very susceptible to pressure and temperature, changes in the marine environment, such as ocean temperature and sea level, may affect the postinjection fate of CO_2 and the efficiency of sequestration. Future work is required to address this topic.

MATERIALS AND METHODS

Different trapping mechanisms correspond to different physical processes. Residual trapping involves the interaction and phase partition of CO_2 and water. Dissolution trapping is related to the distribution of mass components in different phases. Hydrate trapping includes hydrate formation and the consequent effect of permeability reduction, as well as the inhibition of hydrate formation induced by the increasing salinity. The complex process of CO_2 migration in deep-sea sediments can be conceptualized as multiphase, multicomponent, and nonisothermal flow with chemical reaction of hydrate formation and dissociation. Obtaining a precise description of the injection and postinjection fate of CO_2 in marine sediments requires that we fully couple all of these related physics and dynamics. To simulate this multiphysics process, we developed a simulation code for CO_2 sequestration in deep-sea sediments, based on the state-of-art simulation code TOUGH+HYDRATE (*41*), which is used for simulating system behavior in hydrate-bearing geologic media. We maintained the original framework of TOUGH+HYDRATE and incorporated the physical and other related properties of CO_2 into the simulation code; we likewise switched the physical and chemical properties of CH_4 hydrate to CO_2 hydrate. We also modified the primary variable switch method (PVSM) (*41*, *42*) for possible phase changes related to the formation and dissociation of CO_2 hydrate according to the typical conditions of deep-sea sediments. Additional details about the model modification can be found in the Supplementary Materials.

Dealing with multiphase, multicomponent, and nonisothermal flow

Convective fluid flow in porous media is described by Darcy's law, while the diffusion of CO_2 and salt in the aqueous phase is controlled by Fick's

law. The governing equations are essentially mass and energy balance equations. For the CO_2 component, the governing equation is

$$\frac{\partial}{\partial t}\left[\sum_{j=A,L,H}\phi S_j\rho_j X_j^c\right]+\nabla\cdot\left[\sum_{j=A,L,H}\rho_j\vec{v}_j X_j^c+\sum_{j=A,L,H}\vec{J}_j^c\right]=q^c$$

where A, L, and H represent aqueous phase, liquid CO_2 phase, and hydrate phase, respectively; c represents the CO_2 component; ϕ, S, ρ, and X in the first term on the left-hand side are sediment porosity, phase saturation, density, and mass component in a specific phase, respectively; v is phase velocity; J is diffusive mass flow; and q on the right-hand side corresponds to the source and sink term for a specific component. For the water component, the governing equation is

$$\frac{\partial}{\partial t}\left[\sum_{j=A,L,H}\phi S_j\rho_j X_j^w\right]+\nabla\cdot\left[\sum_{j=A,L,H}\rho_j\vec{v}_j X_j^w+\sum_{j=A,L,H}\vec{J}_j^w\right]=q^w$$

where w represents the water component. For the salt component, the governing equation is

$$\frac{\partial}{\partial t}\left[\sum_{j=A,L,H}\phi S_j\rho_j X_j^s\right]+\nabla\cdot\left[\sum_{j=A,L,H}\rho_j\vec{v}_j X_j^s+\sum_{j=A,L,H}\vec{J}_j^s\right]=q^s$$

where s represents the salt component. The final governing equation is the energy balance

$$\frac{\partial}{\partial t}\left[\sum_{j=A,L,H}\phi S_j\rho_j U_j+(1-\phi)\rho_R U_R\right]+$$

$$\nabla\cdot\left[\sum_{j=A,L}\rho_j\vec{v}_j H_j-\lambda\nabla T\right]=q^E$$

where U and H represent internal energy and enthalpy, respectively; the subscript R represents rock; λ and T are thermal conductivity and temperature, respectively; and the superscript E represents energy.

Dealing with potential hydrate formation and dissociation

Since CO_2 hydrate plays an important role in subseabed disposal, the mathematical model needs to incorporate the physical process of hydrate formation and dissociation. CO_2 hydrate appears as the temperature becomes lower than the equilibrium temperature for hydrate formation at prevailing pressure and salinity. Hydrate disappears as its thermodynamic state leaves the zone of hydrate stability or as continuous dissolution of CO_2 occurs from the crystal lattice of hydrate to the surrounding unsaturated aqueous phase accelerated by diffusion and gravity-driven convection. For the chemical reaction of hydrate formation and dissociation, we used the equilibrium reaction model (*43*–*45*), which assumes local thermal and chemical equilibrium for all grid blocks in the numerical model. This hypothesis is reasonable since the time scale of CO_2 transport in marine sediments is much longer than that of the hydrate reaction. The introduction of CO_2 hydrate into the system necessitates an accurate definition of its physical and chemical properties and the way that it affects the properties of the porous sediment, such as effective porosity and permeability. Additional details can be found in the Supplementary Materials.

SUPPLEMENTARY MATERIALS

Supplementary material for this article is available at http://advances.sciencemag.org/cgi/content/full/4/7/eaao6588/DC1

Section S1. Determination of NBZ and HFZ
Section S2. Development of the simulation code for CO_2 sequestration in deep-sea sediments based on TOUGH+HYDRATE
Section S3. Code verification
Section S4. Description of the base case
Fig. S1. Illustration of the NBZ and HFZ with a geothermal gradient of 0.03 K/m, a salinity of 3.5%, and an ocean depth of approximately 3500 m.
Fig. S2. Possible phase changes in the model.
Fig. S3. Phase diagram of CO_2 hydrate.
Fig. S4. Comparison of the analytical Buckley-Leverett solution and the results from the numerical simulation.
Fig. S5. Comparison of the analytical solution and the results from the numerical simulation in the 1D diffusion problem.
Fig. S6. Schematic of the 1D hydrate formation problem.
Fig. S7. Time evolution of pressure at x = 2 m.
Fig. S8. Time evolution of saturation of each phase obtained from the numerical simulation at x = 2 m.
Table S1. Phases and corresponding components in the model.
Table S2. PVSM for CO_2 sequestration in deep-sea sediments.
Table S3. Hydrate-related properties.
Table S4. Physical properties of CO_2 and seawater.
Table S5. Parameter setting for the Buckley-Leverett problem.
Table S6. Parameter setting for 1D diffusion problem.
Table S7. Parameter setting for 1D hydrate formation problem.
Table S8. Parameter setting of the base case.
Table S9. Thermal and hydraulic properties of the formations.
Movie S1. Time evolution of spatial distribution of hydrate saturation in the base case.
Movie S2. Time evolution of spatial distribution of CO_2 saturation in the base case.
Movie S3. Time evolution of spatial distribution of mass fraction of CO_2 in aqueous phase in the base case.
Movie S4. Time evolution of spatial distribution of mass fraction of salt in aqueous phase in the base case.
References (*46*–*64*)

REFERENCES AND NOTES

1. K. S. Lackner, A guide to CO_2 sequestration. *Science* **300**, 1677–1678 (2003).
2. R. K. Pachauri, L. Meyer, G.-K. Plattner, T. Stocker, *IPCC, 2014: Climate Change 2014: Synthesis Report. Contribution of Working Groups I, II and III to the Fifth Assessment Report of the Intergovernmental Panel on Climate Change* (IPCC, 2015).
3. K. Michael, A. Golab, V. Shulakova, J. Ennis-King, G. Allinson, S. Sharma, T. Aiken, Geological storage of CO_2 in saline aquifers—A review of the experience from existing storage operations. *Int. J. Greenh. Gas. Con.* **4**, 659–667 (2010).
4. M. E. Boot-Handford, J. C. Abanades, E. J. Anthony, M. J. Blunt, S. Brandani, N. Mac Dowell, J. R. Fernández, M.-C. Ferrari, R. Gross, J. P. Hallett, R. Stuart Haszeldine, P. Heptonstall, A. Lyngfelt, Z. Makuch, E. Mangano, R. T. J. Porter, M. Pourkashanian, G. T. Rochelle, N. Shah, J. G. Yao, P. S. Fennell, Carbon capture and storage update. *Energ. Environ. Sci.* **7**, 130–189 (2014).
5. B. Metz, O. Davidson, H. De Coninck, M. Loos, L. Meyer, IPCC special report on carbon dioxide capture and storage (Cambridge Univ. Press, 2005).
6. P. G. Brewer, G. Friederich, E. T. Peltzer, F. M. Orr Jr., Direct experiments on the ocean disposal of fossil fuel CO_2. *Science* **284**, 943–945 (1999).
7. P. G. Brewer, E. Peltzer, I. Aya, P. Haugan, R. Bellerby, K. Yamane, R. Kojima, P. Walz, Y. Nakajima, Small scale field study of an ocean CO_2 plume. *J. Oceanogr.* **60**, 751–758 (2004).
8. I. Fer, P. M. Haugan, Dissolution from a liquid CO_2 lake disposed in the deep ocean. *Limnol. Oceanogr.* **48**, 872–883 (2003).
9. H. J. Herzog, E. E. Adams, D. Auerbach, J. Caulfield, Environmental impacts of ocean disposal of CO_2. *Energ. Convers. Manag.* **37**, 999–1005 (1996).
10. H. Koide, Y. Shindo, Y. Tazaki, M. Iijima, K. Ito, N. Kimura, K. Omata, Deep sub-seabed disposal of CO_2—The most protective storage. *Energ. Convers. Manag.* **38**, S253–S258 (1997).
11. J. S. Levine, J. M. Matter, D. Goldberg, A. Cook, K. S. Lackner, Gravitational trapping of carbon dioxide in deep sea sediments: Permeability, buoyancy, and geomechanical analysis. *Geophys. Res. Lett.* **34**, L24703 (2007).
12. K. Z. House, D. P. Schrag, C. F. Harvey, K. S. Lackner, Permanent carbon dioxide storage in deep-sea sediments. *Proc. Natl. Acad. Sci. U.S.A.* **103**, 12291–12295 (2006).

13. D. P. Schrag, Storage of carbon dioxide in offshore sediments. *Science* **325**, 1658–1659 (2009).
14. E. D. Sloan Jr., C. A. Koh, *Clathrate Hydrates of Natural Gases* (CRC Press, ed. 3, 2008).
15. A. Macfarlane, "China makes 'flammable ice' breakthrough in South China Sea" (CNN, 2 August 2017); http://money.cnn.com/2017/05/19/news/china-flammable-ice-sea/index.html.
16. N. Goel, In situ methane hydrate dissociation with carbon dioxide sequestration: Current knowledge and issues. *J. Petrol. Sci. Eng.* **51**, 169–184 (2006).
17. Y. Song, B. Chen, M. Nishio, M. Akai, The study on density change of carbon dioxide seawater solution at high pressure and low temperature. *Energy* **30**, 2298–2307 (2005).
18. B. Tohidi, J. Yang, M. Salehabadi, R. Anderson, A. Chapoy, CO_2 hydrates could provide secondary safety factor in subsurface sequestration of CO_2. *Environ. Sci. Technol.* **44**, 1509–1514 (2010).
19. F. Qanbari, M. Pooladi-Darvish, S. H. Tabatabaie, S. Gerami, CO_2 disposal as hydrate in ocean sediments. *J. Nat. Gas Sci. Eng.* **8**, 139–149 (2012).
20. Q. Li, Z. Wu, X. Li, Prediction of CO_2 leakage during sequestration into marine sedimentary strata. *Energ. Convers. Manag.* **50**, 503–509 (2009).
21. K. Z. House, B. Altundas, C. F. Harvey, D. P. Schrag, The immobility of CO_2 in marine sediments beneath 1500 meters of water. *Chem. Rev.* **3**, 905–912 (2010).
22. C. Rochelle, A. P. Camps, D. Long, A. Milodowski, K. Bateman, D. Gunn, P. Jackson, M. A. Lovell, J. Rees, Can CO_2 hydrate assist in the underground storage of carbon dioxide? *Geol. Soc. Spec. Publ.* **319**, 171–183 (2009).
23. N. Pilisi, D. Ghorbani, S. Vasantharajan, paper presented at the Carbon Management Technology Conference, Orlando, Florida, USA, 7 to 9 February 2012.
24. N. Pilisi, D. Ghorbani, paper presented at the Carbon Management Technology Conference, Orlando, Florida, USA, 7 to 9 February 2012.
25. J. P. Ennis-King, L. Paterson, Role of convective mixing in the long-term storage of carbon dioxide in deep saline formations. *SPE J.* **10**, 349–356 (2005).
26. X. Xu, S. Chen, D. Zhang, Convective stability analysis of the long-term storage of carbon dioxide in deep saline aquifers. *Adv. Water Resour.* **29**, 397–407 (2006).
27. S. Rapaka, S. Chen, R. J. Pawar, P. H. Stauffer, D. Zhang, Non-modal growth of perturbations in density-driven convection in porous media. *J. Fluid Mech.* **609**, 285–303 (2008).
28. K. Pruess, K. Zhang, *Numerical Modeling Studies of The Dissolution-Diffusion-Convection Process during CO_2 Storage in Saline Aquifers* (Lawrence Berkeley National Laboratory, 2008).
29. S. Chevalier, T. F. Faisal, Y. Bernabe, R. Juanes, M. Sassi, Numerical sensitivity analysis of density driven CO_2 convection with respect to different modeling and boundary conditions. *Heat Mass Transf.* **51**, 941–952 (2015).
30. X. Liu, P. B. Flemings, Passing gas through the hydrate stability zone at southern Hydrate Ridge, offshore Oregon. *Earth. Planet. Sci. Lett.* **241**, 211–226 (2006).
31. X. Liu, P. B. Flemings, Dynamic multiphase flow model of hydrate formation in marine sediments. *J. Geophys. Res.* **112**, B03101 (2007).
32. H. Deng, P. Stauffer, Z. Dai, Z. Jiao, R. C. Surdam, Simulation of industrial-scale CO_2 storage: Multi-scale heterogeneity and its impacts on storage capacity, injectivity and leakage. *Int. J. Greenh. Gas Con.* **10**, 397–418 (2012).
33. M. Flett, R. Gurton, G. Weir, Heterogeneous saline formations for carbon dioxide disposal: Impact of varying heterogeneity on containment and trapping. *J. Petrol. Sci. Eng.* **57**, 106–118 (2007).
34. U. Lengler, M. De Lucia, M. Kühn, The impact of heterogeneity on the distribution of CO_2: Numerical simulation of CO_2 storage at Ketzin. *Int. J. Greenh. Gas Con.* **4**, 1016–1025 (2010).
35. H. R. Jahangiri, D. Zhang, Effect of spatial heterogeneity on plume distribution and dilution during CO_2 sequestration. *Int. J. Greenh. Gas Con.* **5**, 281–293 (2011).
36. C. P. Green, J. Ennis-King, Effect of vertical heterogeneity on long-term migration of CO_2 in saline formations. *Trans. Porous Media* **82**, 31–47 (2010).
37. W. A. Ambrose, S. Lakshminarasimhan, M. H. Holtz, V. Núñez-López, S. D. Hovorka, I. Duncan, Geologic factors controlling CO_2 storage capacity and permanence: Case studies based on experience with heterogeneity in oil and gas reservoirs applied to CO_2 storage. *Environ. Geol.* **54**, 1619–1633 (2008).
38. E. Lindeberg, Escape of CO_2 from aquifers. *Energ. Convers. Manag.* **38**, S235–S240 (1997).
39. E. Saadatpoor, S. L. Bryant, K. Sepehrnoori, New trapping mechanism in carbon sequestration. *Trans. Porous Media* **82**, 3–17 (2010).
40. S. C. M. Krevor, R. Pini, B. Li, S. M. Benson, Capillary heterogeneity trapping of CO_2 in a sandstone rock at reservoir conditions. *Geophys. Res. Lett.* **38**, L15401 (2011).
41. G. J. Moridis, M. B. Kowalsky, K. Pruess, *TOUGH+ HYDRATE v1. 2 User's Manual: A Code for the Simulation of System Behavior in Hydrate-Bearing Geologic Media* (Lawrence Berkeley National Laboratory, 2014).
42. X. Sun, K. K. Mohanty, Kinetic simulation of methane hydrate formation and dissociation in porous media. *Chem. Eng. Sci.* **61**, 3476–3495 (2006).
43. M. B. Kowalsky, G. J. Moridis, Comparison of kinetic and equilibrium reaction models in simulating gas hydrate behavior in porous media. *Energ. Convers. Manag.* **48**, 1850–1863 (2007).
44. I. K. Gamwo, Y. Liu, Mathematical modeling and numerical simulation of methane production in a hydrate reservoir. *Ind. Eng. Chem. Res.* **49**, 5231–5245 (2010).
45. Y. Liu, I. K. Gamwo, Comparison between equilibrium and kinetic models for methane hydrate dissociation. *Chem. Eng. Sci.* **69**, 193–200 (2012).
46. R. Span, W. Wagner, A new equation of state for carbon dioxide covering the fluid region from the triple-point temperature to 1100 K at pressures up to 800 MPa. *J. Phys. Chem. Ref. Data.* **25**, 1509–1596 (1996).
47. X. Sun, K. K. Mohanty, paper presented at the 2005 SPE Reservoir Simulation Symposium, Houston, Texas, USA, 31 January to 2 February 2005.
48. G. R. Dickens, M. S. Quinby-Hunt, Methane hydrate stability in pore water: A simple theoretical approach for geophysical applications. *J. Geophys. Res. Atmos.* **102**, 773–783 (1997).
49. "Gas Hydrates for Deep Ocean Storage of CO_2" (Report no. PH4/26, IEA Greenhouse Gas R&D Programme, 2004); http://ieaghg.org/docs/General_Docs/Reports/PH4-26%20CO2%20hydrates.pdf.
50. L. W. Diamond, N. N. Akinfiev, Solubility of CO_2 in water from −1.5 to 100 degrees C and from 0.1 to 100 MPa: Evaluation of literature data and thermodynamic modelling. *Fluid Phase Equilib.* **208**, 265–290 (2003).
51. N. N. Akinfiev, L. W. Diamond, Thermodynamic model of aqueous CO_2–H_2O–NaCl solutions from−22 to 100°C and from 0.1 to 100 MPa. *Fluid. Phase. Equilib.* **295**, 104–124 (2010).
52. A. Fenghour, W. A. Wakeham, V. Vesovic, The viscosity of carbon dioxide. *J. Phys. Chem. Ref. Data.* **27**, 31–44 (1998).
53. J. W. Mutoru, A. Leahy-Dios, A. Firoozabadi, Modeling infinite dilution and Fickian diffusion coefficients of carbon dioxide in water. *AIChE J.* **57**, 1617–1627 (2011).
54. W. M. Haynes, *CRC Handbook of Chemistry and Physics* (CRC Press, ed. 95, 2014).
55. F. J. Millero, F. Huang, The density of seawater as a function of salinity (5 to 70 g kg^{-1}) and temperature (273.15 to 363.15 K). *Ocean. Sci.* **5**, 91–100 (2009).
56. K. Pruess, The TOUGH codes—A family of simulation tools for multiphase flow and transport processes in permeable media. *Vadose Zone J.* **3**, 738–746 (2004).
57. G. J. Moridis, K. Pruess, T2SOLV: An enhanced package of solvers for the TOUGH2 family of reservoir simulation codes. *Geothermics* **27**, 415–444 (1998).
58. K. Pruess, A. Simmons, Y. Wu, G. Moridis, "TOUGH2 software qualification" (Report no. LBL-38383, Lawrence Berkeley Lab and Geological Survey, 1996).
59. G. J. Moridis, T. S. Collett, R. Boswell, M. Kurihara, M. T. Reagan, C. Koh, E. D. Sloan, Toward production from gas hydrates: Current status, assessment of resources, and simulation-based evaluation of technology and potential. *SPE Reservoir Eval. Eng.* **12**, 745–771 (2009).
60. G. J. Moridis, T. S. Collett, S. R. Dallimore, T. Inoue, T. Mroz, Analysis and interpretation of the thermal test of gas hydrate dissociation in the JAPEX/JNOC/GSC et al. Mallik 5L-38 gas hydrate production research well, in *Scientific Results From the Mallik 2002 Gas Hydrate Production Research Well Program, Mackenzie Delta, Northwest Territories*, S. R. Dallimore, T. S. Collett, Eds. (Geological Survey of Canada, 2005), p. 585.
61. L.-G. Tang, X.-S. Li, Z.-P. Feng, G. Li, S.-S. Fan, Control mechanisms for gas hydrate production by depressurization in different scale hydrate reservoirs. *Energy Fuel* **21**, 227–233 (2007).
62. S. E. Buckley, M. C. Leverett, Mechanism of fluid displacement in sands. *Trans. AIME* **146**, 107–116 (1942).
63. G. J. Moridis, Y. Seol, T. J. Kneafsey, *Studies of Reaction Kinetics of Methane Hydrate Dissociation in Porous Media* (Lawrence Berkeley National Laboratory, 2005).
64. W.-J. Plug, J. Bruining, Capillary pressure for the sand–CO_2–water system under various pressure conditions. Application to CO_2 sequestration. *Adv. Water. Resour.* **30**, 2339–2353 (2007).

Acknowledgments

Funding: This work was partially funded by the Peking University carbon capture, utilization and storage project supported by BHP Billiton. **Author contributions:** D.Z. and Y.T. conceived the study and wrote the paper together. Y.T. developed the coupled multiphysics model and conducted simulations. Y.T. and D.Z. designed study cases and analyzed and interpreted results. **Competing interests:** The authors declare that they have no competing interests. **Data and materials availability:** All data needed to evaluate the conclusions in the paper are present in the paper and/or the Supplementary Materials. Additional data related to this paper may be requested from the authors.

Submitted 12 August 2017
Accepted 22 May 2018
Published 4 July 2018
10.1126/sciadv.aao6588

Citation: Y. Teng, D. Zhang, Long-term viability of carbon sequestration in deep-sea sediments. *Sci. Adv.* **4**, eaao6588 (2018).

ScienceAdvances

Long-term viability of carbon sequestration in deep-sea sediments

Yihua Teng and Dongxiao Zhang

Sci Adv **4** (7), eaao6588.
DOI: 10.1126/sciadv.aao6588